JOURNAL OF GUIDANCE, CONTROL, AND DYNAMICS
Vol. 26, No. 6, November–December 2003

Constrained Circularization in Elliptic Orbit Using Low Thrust with Shadowing Effect

Jean A. Kéchichian*
The Aerospace Corporation, El Segundo, California 90245-4691

The optimal thrust pitch angle variation that results in the maximum change in the eccentricity in general elliptic orbit using continuous, constant, low-thrust acceleration while keeping the orbit energy unchanged after a full thrust cycle is determined by direct use of the theory of maxima and through numerical quadrature and search techniques. The analysis takes into account the presence of a shadow arc arbitrarily positioned along the elliptic orbit, where thrust is cut off. Unlike the well-known nonoptimal scheme that uses a thrust orientation perpendicular to the line of apsides at all times, the present optimal scheme allows for the maximum change in eccentricity for a more efficient orbit circularization. Approximate but highly accurate analytic expressions for the changes in the eccentricity and semimajor axis of a general elliptic orbit, perturbed by a constant low-thrust acceleration applied along the fixed inertial direction normal to the orbit major axis, are also derived for general use and rapid calculations.

Introduction

THE problem of the maximization of the change in the eccentricity of a general elliptic orbit using continuous constant low-thrust acceleration while constraining the semimajor axis a to stay constant after one full cycle of thrust is analyzed, by also taking into account the presence of the Earth shadow arc where the thrust is turned off. Elliptic orbit circularization with electric thrusters is presently performed by geostationary communications spacecraft that are initially released into highly elliptic supersynchronous orbits, subsequently circularized by also maintaining orbital energy constant.

The optimization method is similar to the one used in Refs. 1–3, which was also applied in Ref. 4 under the same assumption of the initially circular orbit model. In particular, in Refs. 2 and 3, the problem of transferring a spacecraft between two inclined circular orbits, of different size and inclination, in minimum time, using discontinuous low-thrust acceleration is considered. The two-body thrust-perturbed orbit is, thus, constrained to remain circular during the transfer, and the optimal control law for the thrust direction derived for the fast timescale problem of maximizing the inclination change for a given change in the semimajor axis is used in an averaging procedure to solve the overall slow timescale transfer problem. The present paper tackles the fast timescale planar problem in the more general elliptic case, by deriving the optimal thrust pitch profile that maximizes the change in eccentricity without changing semimajor axis and by also extending the analysis to the dual problem of maximizing the orbit semimajor axis while keeping the eccentricity e unchanged after one cycle of intermittent thrust. The change in eccentricity over a single orbit can then be used in conjunction with an inclination change to produce averaged rates of change in the eccentricity and inclination to solve the overall slow timescale minimum-time transfer problem of circularizing and rotating an initial elliptic orbit without changing its orbital energy. The theory of maxima is, thus, employed in the present planar problem, and the value of a certain constant Lagrange multiplier is determined numerically by way of an iterative scheme such that the corresponding integral constraint evaluated by numerical quadrature is driven to zero. The optimal thrust vector pitch angle is then obtained as a direct function of the orbital position of the spacecraft, which is selected here as the true anomaly. Simple orbit circularization schemes are proposed in Refs. 5–7 for the continuous thrust case. Spitzer[6,7] adopts the inertially fixed firing orientation where the thrust is applied perpendicular to the line of apsides providing near-optimal results while also ensuring semimajor axis constancy to first order, in the process.

The presence of a shadow arc disrupts the constancy of the semimajor axis when the inertially fixed firing direction mode is used. The optimal mode derived here by extending the results obtained in the circular case[8] ensures that the tailored thrust-pitch profile not only optimizes the change in the eccentricity but also satisfies the semimajor axis constraint regardless of the size and orbital location of the shadow arc.

Finally, analytic integrations of the differential equations for the variables a and e, which consist of the variational equations of the orbit, are carried out using the inertially fixed firing scheme in the elliptic case, so that the changes in a and e are easily evaluated from their corresponding approximate analytic expressions, valid for about one revolution about the central body, without the need to integrate the differential equations numerically.

Maximization of the Change in Eccentricity Subject to Zero Change in the Semimajor Axis for Discontinuous Thrusting in Elliptic Orbit

Figure 1 shows an elliptic orbit with the Earth–sun line contained in the orbit plane, yielding the worst-case shadowing represented by the arc $E'H'$ where no thrust is applied. The thrust-pitch angle α is the angle between the radial direction $\hat{r}$ and the thrust vector $\boldsymbol{T}$, and θ_1^* and θ_2^* are the true anomalies of the shadow entry and exit points E' and H', respectively. The Earth–sun line is inclined at an angle β with respect to the eccentricity vector orientation, with the sunlight cylinder tangent to the Earth sphere intersecting the orbit at four distinct locations, E, H, and E', H'. Letting $R_\oplus = 6378.14$ km represent the Earth radius, the equations of the lines EE' and HH' are given, respectively, by

$$y = (x - ae)\tan\beta + R_\oplus / c_\beta \tag{1}$$

$$y = (x - ae)\tan\beta - R_\oplus / c_\beta \tag{2}$$

with x along $\boldsymbol{e}$ and y along the semiminor axis, where c_β is used for $\cos\beta$, etc., and a and b are the orbit semimajor axis and semiminor

Received 3 June 2002; presented as Paper 2002-4894 at the AIAA/AAS Astrodynamics Specialist Conference, Monterey, CA, 5–8 August 2002; revision received 17 June 2003; accepted for publication 17 June 2003.

*Engineering Specialist, Astrodynamics Department, Mail Stop M4-947, P.O. Box 92957, Los Angeles, CA 90009; JeanA.Kechichian@aero.org.

Table 1 Shadow entry and exit true anomalies vs β for worst-case shadowing with $a = 40{,}000$ km and $e = 0.7$

	β, deg					
Anomaly	*0 (180)*	*30 (210)*	*60 (240)*	*90 (270)*	*120 (300)*	*150 (330)*
θ_0^*, deg	*185.438741*	*218.068229*	*254.786809*	*293.593947*	*330.165966*	*2.097728*
	(30.128698)	*(55.823269)*	*(80.428847)*	*(104.863308)*	*(129.916827)*	*(156.433484)*
θ_f^*, deg	*534.561259*	*563.566516*	*590.083173*	*615.136692*	*639.571153*	*304.176731*
	(329.871302)	*(357.902271)*	*(389.834034)*	*(426.406053)*	*(465.213191)*	*(509.931771)*

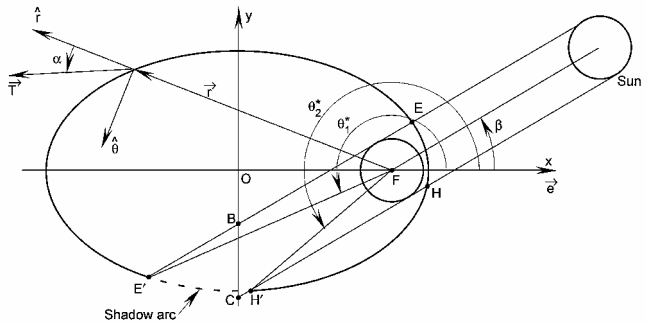

Fig. 1 Shadowing geometry on elliptic orbit.

axis, respectively. The coordinates of the points H and H' are obtained by substituting y from Eq. (2) into the equation of the ellipse, namely, $x^2/a^2 + y^2/b^2 = 1$, and solving for the two values of x from the resulting quadratic $Ax^2 + Bx + C = 0$, where

$$C = D - 1, \qquad A = 1/a^2 + \tan^2\beta/b^2$$

$$B = -\left[2ae\tan^2\beta + 2(R_\oplus/c_\beta)\tan\beta\right]\Big/b^2$$

$$D = (1/b^2)(R_\oplus/c_\beta + ae\tan\beta)^2$$

The coordinates of the intersection points of the line EE' with the ellipse are obtained likewise using Eq. (1) and solving for the value of x from the quadratic $Ax^2 + B'x + C'$ with $C' = D' - 1$ and

$$B' = -\left[2ae\tan^2\beta - 2(R_\oplus/c_\beta)\tan\beta\right]\Big/b^2$$

$$D' = (1/b^2)(R_\oplus/c_\beta - ae\tan\beta)^2$$

For $\beta = 90$ and 270 deg, the lines HH' and EE' are described by the equations $x = ae + R_\oplus$ and $x = ae - R_\oplus$, respectively, for $\beta = 90$ deg, or the converse for $\beta = 270$ deg, such that the four intersection points are now obtained by inserting these expressions for x in the equation of the ellipse and solving for the values of y, respectively, as

$$y = \pm\left[b^2 - (b^2/a^2)(ae + R_\oplus)^2\right]^{\frac{1}{2}}$$

$$y = \pm\left[b^2 - (b^2/a^2)(ae - R_\oplus)^2\right]^{\frac{1}{2}}$$

Because $x = ac_E$ and $y = bs_E$, the value of the eccentric anomaly E is readily obtained from the coordinates x and y, and finally, the true anomaly of each intersection point is known from the identities

$$s_{\theta^*} = \frac{(1-e^2)^{\frac{1}{2}}s_E}{(1-ec_E)}, \qquad c_{\theta^*} = \frac{(c_E - e)}{(1-ec_E)}$$

Thus, for a given sun angle β, the true anomalies of the shadow entry and exit points, θ_1^* and θ_2^*, respectively, are easily obtained.

These angles are displayed in Table 1 for various β angles covering the whole range $0 \le \beta \le 360$ deg with θ_0^* standing for θ_2^* and θ_f^* standing for θ_1^* and where an angle of 360 deg has been added to θ_f^* where needed, such that the thrust is applied from θ_0^* (shadow exit) to θ_f^* (shadow entry) with the angle always increasing for reliable integration.

When $k = T/m$ is the constant thrust acceleration magnitude, the $\hat{\boldsymbol{r}}$ and $\hat{\boldsymbol{\theta}}$ components of this acceleration, namely, f_r and f_θ, are given by kc_α and ks_α, respectively. Here $\hat{\boldsymbol{r}}$ and $\hat{\boldsymbol{\theta}}$ are unit vectors along the radial direction and the direction 90 deg ahead of it, such that the differential equations valid in elliptic orbit are given by[9]

$$\dot{a} = \frac{2es_{\theta^*}}{n(1-e^2)^{\frac{1}{2}}}f_r + \frac{2(1+ec_{\theta^*})}{n(1-e^2)^{\frac{1}{2}}}f_\theta \tag{3}$$

$$\dot{e} = \frac{(1-e^2)^{\frac{1}{2}}}{na}s_{\theta^*}f_r + \frac{(1-e^2)^{\frac{1}{2}}}{nae}\left(1 + ec_{\theta^*} - \frac{1-e^2}{1+ec_{\theta^*}}\right)f_\theta \tag{4}$$

where n represents the orbit mean motion $\mu^{1/2}a^{-3/2}$. Because the thrust acceleration magnitude is very low, we can neglect the contributions of the terms in f_r and f_θ in the differential equation for θ^*

$$\frac{\mathrm{d}\theta^*}{\mathrm{d}t} = \frac{h}{r^2} - \frac{r}{he}[-c_{\theta^*}(1+ec_{\theta^*})f_r + s_{\theta^*}(2+ec_{\theta^*})f_\theta]$$

such that this general singular form is reduced to the following simple form:

$$\frac{\mathrm{d}\theta^*}{\mathrm{d}t} = \frac{h}{r^2} = \frac{n(1+ec_{\theta*})^2}{(1-e^2)^{\frac{3}{2}}} \tag{5}$$

after replacement of h and r by $\mu^{1/2}a^{1/2}(1-e^2)^{1/2}$ and $a(1-e^2)/(1+ec_{\theta^*})$, respectively. Equations (3) and (4) are now written in terms of θ^* (the independent variable instead of t, the physical time) after division by Eq. (5), such that the following approximate form is obtained:

$$\frac{\mathrm{d}a}{\mathrm{d}\theta^*} = \frac{2es_{\theta^*}(1-e^2)}{n^2(1+ec_{\theta^*})^2}kc_\alpha + \frac{2(1-e^2)}{n^2(1+ec_{\theta^*})}ks_\alpha \tag{6}$$

$$\frac{\mathrm{d}e}{\mathrm{d}\theta^*} = \frac{(1-e^2)^2 s_{\theta^*}}{n^2a(1+ec_{\theta^*})^2}kc_\alpha + \frac{(1-e^2)^2}{n^2ae} \times \left[\frac{1}{1+ec_{\theta*}} - \frac{(1-e^2)}{(1+ec_{\theta*})^3}\right]ks_\alpha \tag{7}$$

The changes Δa and Δe over one revolution can be written as follows as a result of applying the low-thrust acceleration between θ_0^* and θ_f^*:

$$\Delta a = \frac{2(1-e^2)k}{n^2}\int_{\theta_0^*}^{\theta_f^*}\left[\frac{es_{\theta^*}c_\alpha}{(1+ec_{\theta^*})^2} + \frac{s_\alpha}{(1+ec_{\theta^*})}\right]\mathrm{d}\theta^* \tag{8}$$

$$\Delta e = \frac{(1-e^2)^2 k}{n^2a} \times \int_{\theta_0^*}^{\theta_f^*}\left[\frac{s_{\theta*}c_\alpha}{(1+ec_{\theta*})^2} + \frac{s_\alpha}{e(1+ec_{\theta*})} - \frac{(1-e^2)s_\alpha}{e(1+ec_{\theta*})^3}\right]\mathrm{d}\theta^* \tag{9}$$

To maximize the change in e, namely, Δe, subject to the constraint $\Delta a = 0$, the following augmented integral is formed with the use of the constant Lagrange multiplier λ that effectively adjoins Δa to

the preceding Δe expression, namely, $I(\alpha) = \Delta e + \lambda \Delta a$,

$$I(\alpha) = \int_{\theta_0^*}^{\theta_f^*} \frac{(1-e^2)k}{n^2} \left\{ \frac{(1-e^2)}{a} \left[\frac{s_{\theta^*} c_\alpha}{(1+ec_{\theta*})^2} + \frac{s_\alpha}{e(1+ec_{\theta^*})} \right.\right.$$

$$\left.\left. - \frac{(1-e^2)s_\alpha}{e(1+ec_{\theta^*})^3} \right] + 2\lambda \left[\frac{e s_{\theta^*} c_\alpha}{(1+ec_{\theta^*})^2} + \frac{s_\alpha}{(1+ec_{\theta^*})} \right] \right\} \mathrm{d}\theta^* \quad (10)$$

Let F stand for the preceding integrand, then Euler's equation $\partial F/\partial \alpha = 0$, which is a necessary condition for optimality, provides the optimal thrust pitch law as

$$\tan\alpha = \left\{ (1-e^2)\left[(1+ec_{\theta^*})^2 - (1-e^2) \right] + 2ae\lambda (1+ec_{\theta^*})^2 \right\} \Big/$$

$$e(1+ec_{\theta^*})\left[(1-e^2) + 2ae\lambda \right] s_{\theta^*} \quad (11)$$

This expression yields in turn

$$s_\alpha^2 = \left\{ -(1-e^2)\left[(1+ec_{\theta^*})^2 - (1-e^2) \right] - 2ae\lambda (1+ec_{\theta^*})^2 \right\}^2 \Big/ X$$

$$c_\alpha^2 = e^2 (1+ec_{\theta^*})^2 \left[-(1-e^2)s_{\theta^*} - 2ae\lambda s_{\theta^*} \right]^2 \Big/ X$$

where X is given by

$$X = e^2 (1+ec_{\theta^*})^2 \left[-(1-e^2)s_{\theta^*} - 2ae\lambda s_{\theta^*} \right]^2$$

$$+ \left\{ -(1-e^2)\left[(1+ec_{\theta^*})^2 - (1-e^2) \right] - 2ae\lambda (1+ec_{\theta^*})^2 \right\}^2$$

Using these expressions of s_α and c_α in Eq. (8) for Δa results in the following integral after carrying out some manipulations:

$$\Delta a = \frac{2(1-e^2)k}{n^2} \times \int_{\theta_0^*}^{\theta_f^*} \frac{[-(1-e^2) - 2ae\lambda](1+e^2+2ec_{\theta^*}) + (1-e^2)^2}{(1+ec_{\theta^*})X^{\frac{1}{2}}} \mathrm{d}\theta^* \quad (12)$$

The value of λ is searched on and the integral constraint (12) evaluated each time by numerical quadrature between the limits θ_0^* and θ_f^* where the thrust is on, until the value of Δa is driven to zero to within a small tolerance. A 10-point Gauss–Legendre quadrature (see Ref. 10) of the Δa integral is performed, and the zero crossing of the Δa function is established, such that the Wijngaarden–Dekker–Brent method (see Ref. 10), which consists of combining root bracketing, bisection, and inverse quadratic interpolation, is used to zero in on the exact value of λ from the zero crossing neighborhood. For the example orbit of Table 1, λ is of the order of -10^{-6} 1/km, and for the dual problem of maximizing Δa with zero Δe change, λ is of the order of 10^5 km. Once λ is determined, the angle α that maximizes the change in the eccentricity Δe is obtained from Eq. (11) such that Δe itself is now determined by numerical quadrature from Eq. (9), namely,

$$\Delta e = \frac{(1-e^2)^2 k}{n^2 a} \times \int_{\theta_0^*}^{\theta_f^*} \left[\frac{s_{\theta^*} c_\alpha}{(1+ec_{\theta^*})^2} + \frac{s_\alpha}{e(1+ec_{\theta^*})} - \frac{(1-e^2)s_\alpha}{e(1+ec_{\theta^*})^3} \right] \mathrm{d}\theta^* \quad (13)$$

Because of the squaring operations, the preceding s_α^2 and c_α^2 expressions provide s_α and c_α with the plus or minus sign. In as much as both signs must be either plus or minus, because otherwise the $\tan\alpha$ expression will change sign, the λ value that drives Δa to zero is the same in either case. However, the plus sign will yield Δe with the pitch angle α, with Δe being either positive or negative, and the minus sign will yield the same Δe with the opposite sign, using the thrust pitch angle $\alpha + \pi$, because in the latter case the thrust direction is exactly opposite to the direction that corresponds to the selection of the plus sign. In other words, if Δe is positive with the plus sign selected for the s_α and c_α expressions, then it will be negative with the minus sign selection and vice versa. If the constraint $\Delta a = 0$ is not enforced, then the maximization of Δe in elliptic orbit is made possible by simply setting $\lambda = 0$ in Eq. (11) resulting in the optimal law

$$\tan\alpha = \frac{(1+ec_{\theta^*})^2 - (1-e^2)}{e(1+ec_{\theta^*})s_{\theta^*}} \quad (14)$$

This angle α also maximizes in this case, the instantaneous rate of change of e. In the circular case, the limit as $e \to 0$ of expression (14) will be given by[1]

$$\tan\alpha = 2/\tan\theta^* \quad (15)$$

which is the well-known optimal thrust steering program to maximize Δe from an initially circular orbit. In practice when e is near zero, the nonzero average e over one revolution is to be used instead, and θ^* is just the angular position measured from the shadow exit point with $\theta_0^* = 0$.

The case that corresponds to $\beta = 180$ deg is now solved with $\theta_0^* = 30.128698$ deg, $\theta_f^* = 329.871302$ deg using $k = 3.5 \times 10^{-7}$ km/s^2 for the constant thrust acceleration and an initial orbit given by $a = 40{,}000$ km and $e = 0.7$ yielding $\lambda = -0.445453 \times 10^{-6}$ 1/km, and a corresponding Δe from Eq. (13) of $-0.9042309 \times 10^{-2}$. Equations (6) and (7) are now integrated numerically from the initial state using $\alpha = f(\theta^*)$ from Eq. (11) and holding a, e, and n constant in the right-hand side of each of the two differential equations, starting from θ_0^* until θ_f^*. This verification run yields the final state $a_f = 40{,}005.308$ km and $e_f = 0.69060484$, which corresponds to an achieved $(\Delta e)_f$ of $-0.9395152 \times 10^{-2}$.

Maximization of the Change in Semimajor Axis Subject to Zero Change in the Eccentricity for Discontinuous Thrust in Elliptic Orbit

The dual problem of maximizing the orbit energy subject to the constraint $\Delta e = 0$ is carried out by forming the following augmented integral, namely, $I(\alpha) = \Delta a + \lambda \Delta e$:

$$I(\alpha) = \frac{(1-e^2)k}{n^2} \int_{\theta_0^*}^{\theta_f^*} \left\{ 2\left[\frac{e s_{\theta^*} c_\alpha}{(1+ec_{\theta^*})^2} + \frac{s_\alpha}{(1+ec_{\theta^*})} \right] + \frac{\lambda(1-e^2)}{a} \right.$$

$$\left. \times \left[\frac{s_{\theta^*} c_\alpha}{(1+ec_{\theta^*})^2} + \frac{s_\alpha}{e(1+ec_{\theta^*})} - \frac{(1-e^2)s_\alpha}{e(1+ec_{\theta^*})^3} \right] \right\} \mathrm{d}\theta^* \quad (16)$$

When F stands for the integrand in Eq. (16), the optimal pitch angle α is obtained as a function of θ^* and the multiplier λ by direct application of the Euler equation as before, $\partial F/\partial\alpha = 0$, leading to

$$\tan\alpha = \frac{\lambda(1-e^2)\left[(1+ec_{\theta^*})^2 - (1-e^2) \right] + 2ae(1+ec_{\theta^*})^2}{e(1+ec_{\theta^*})\left[\lambda(1-e^2) + 2ae \right] s_{\theta^*}} \quad (17)$$

If the $\Delta e = 0$ constraint is not enforced, then $\lambda = 0$ is selected in Eq. (17) for the pitch profile that would maximize Δa for the unconstrained elliptic case resulting in

$$\tan\alpha = \frac{(1+ec_{\theta^*})}{e s_{\theta^*}} \quad (18)$$

However, the flight direction angle γ, which is the angle between the radius vector $\boldsymbol{r}$ and the velocity vector $\boldsymbol{v}$, is given by[9]

$$s_\gamma = (\mu/h\upsilon)(1+ec_{\theta^*}), \qquad c_\gamma = (\mu/h\upsilon)e s_{\theta^*}$$

where h is the orbital angular momentum, such that

$$\tan\gamma = \frac{(1+ec_{\theta^*})}{e s_{\theta^*}} \quad (19)$$

which is identical to Eq. (18). Thus, $\alpha = \gamma$, and the thrust vector is then aligned with the velocity vector itself, which is the well-known solution for maximizing the orbit semimajor axis in the unconstrained elliptic case. In the limiting case where e approaches zero, $\tan\alpha$ will tend to ∞ and α to 90 deg, again pointing the thrust vector along the velocity vector.

Return to the constrained case, Eq. (17) yields

$$s_\alpha^2 = \left\{(1-e^2)\left[\lambda(1+ec_{\theta^*})^2 - \lambda(1-e^2)\right] + 2ae(1+ec_{\theta^*})^2\right\}^2 \Big/ X'$$

$$c_\alpha^2 = e^2(1+ec_{\theta^*})^2\left[\lambda(1-e^2)s_{\theta^*} + 2aes_{\theta^*}\right]^2 \Big/ X'$$

where X' is the sum of the squares of the numerator and denominator in the $\tan\alpha$ expression. The same discussion concerning the sign of s_α and c_α made in the preceding section also applies here. With replacement in the Δe expression in Eq. (9), the following form for that integral is obtained after some manipulations:

$$\Delta e = \frac{(1-e^2)^2 k}{n^2 ae} \times \int_{\theta_0^*}^{\theta_f^*} \left\{ \frac{\left[\lambda(1-e^2)+2ae\right]\left(2e^2+2ec_{\theta^*}\right) - \lambda(1-e^2)^2}{(1+ec_{\theta^*})X'^{\frac{1}{2}}} + \frac{\lambda(1-e^2)^3}{(1+ec_{\theta^*})^3 X'^{\frac{1}{2}}} \right\} d\theta^* \tag{20}$$

As before, the value of λ is searched on and the preceding integral evaluated by numerical quadrature between the bounds θ_0^* and θ_f^*, where the thrust is on, until $\Delta e = 0$ is achieved to within a small tolerance.

Δa is then obtained from Eq. (8) also by quadrature once λ is determined, and α is made a function of the constants a and e and the integration variable θ^* only, in Eq. (17).

The example initial orbit of the preceding section is used, and the following optimal solution that maximizes Δa is obtained, namely, $\lambda = 0.20597067506 \times 10^5$ km with $\Delta a = 545.016$ km and with integrated a_f and e_f using Eqs. (6) and (7), of 40,529.360 km and 0.699020655, respectively. The two optimal solutions, namely, the Δe and Δa-maximized thus generated, are now compared to the simple nonoptimal Spitzer firing scheme,[6,7] where the thrust vector is directed along a direction normal to the orbit line of apsides resulting in an inertially fixed firing mode. In this scheme $c_\alpha = -s_{\theta^*}$ and $s_\alpha = -c_{\theta^*}$ will effectively decrease the orbit eccentricity, whereas $c_\alpha = s_{\theta^*}$ and $s_\alpha = c_{\theta^*}$ will increase it, with the first mode firing opposite the velocity vector at perigee and along the velocity vector at apogee effectively lowering apogee and raising perigee to decrease e and the second mode giving exactly the reverse result. With use of the first Spitzer mode, to lower eccentricity, the initial orbit is integrated using Eqs. (6) and (7) between $\theta_0^* = 30.128698$ and $\theta_f^* = 329.871302$ deg as for the two preceding optimal cases, yielding $a_f = 40{,}035.843$ km, and $e_f = 0.690812921$, with the latter value slightly higher than the one generated by the Δa-constrained, maximum e-drop solution at $e_f = 0.69060484$; a_f itself is larger than the desired value of 40,000 km in this case because the Spitzer modes cannot constrain the energy of the orbit.

Figures 2–4 show the pitch angle, semimajor axis, and eccentricity variations, respectively, of the two constrained optimal solutions, as well as the Spitzer[6,7] solution, showing how the first Spitzer firing mode is nearly identical to the optimal mode that maximizes the drop in e. Unlike these two modes that display a sign change in α to accelerate and decelerate the vehicle along its orbit, the maximum Δa solution keeps a positive α value throughout. Figure 3 shows how the Spitzer mode fails to recover the initial semimajor axis after one cycle of thrust even though it matches closely the optimal Δe change as shown in Fig. 4.

Further Numerical Comparisons

A series of runs is now made for various values of sun angle β using both the constrained Δe-maximizing strategy and the Spitzer[6,7] strategy, with the shadow exit and entry true anomalies in Table 1 for each corresponding β angle. Tables 2 and 3 show the values of the iterated multiplier λ, as well as the $(\Delta e)_{\Delta e}$ computed from the Δe integral by quadrature, and the numerically integrated $(a_f)_{\Delta e}$ and $(e_f)_{\Delta e}$ final parameters of the optimized solutions for each β. The $(a_f)_s$ and $(e_f)_s$ of the Spitzer integrated trajectories are also shown in Tables 2 and 3 with $(a_f)_s$, undershooting the desired 40,000-km mark in the range $\beta = 330$–30 deg and overshooting in the much wider range of $60 < \beta < 300$ deg. When β is either 0 or 180 deg, that is, when the Earth–sun line is along the orbit line of apsides, the shadow arcs are centered at the orbit apogee and perigee, respectively, resulting in higher variations of $(a_f)_s$ from the 40,000-km value, which is by contrast fairly well matched by the constrained solutions as shown in Tables 2 and 3 to within a few kilometers only.

A higher-order quadrature method than the 10-point Legendre–Gauss method used here might more closely enforce the $\Delta a = 0$ constraint. Nevertheless, Fig. 5 shows both $(a_f)_{\Delta e}$ and $(a_f)_s$ values as a function of β for the entire range $0 < \beta < 360$ deg with the

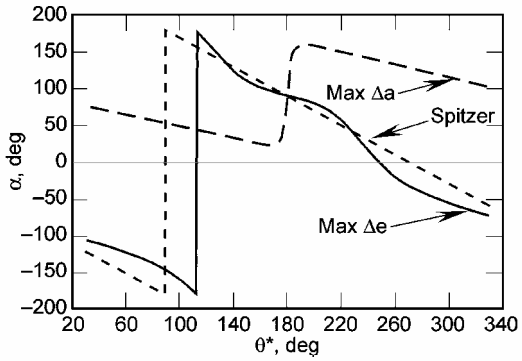

Fig. 2 Thrust-pitch angle variation for maximum Δe, maximum Δa, and Spitzer[6,7] solutions.

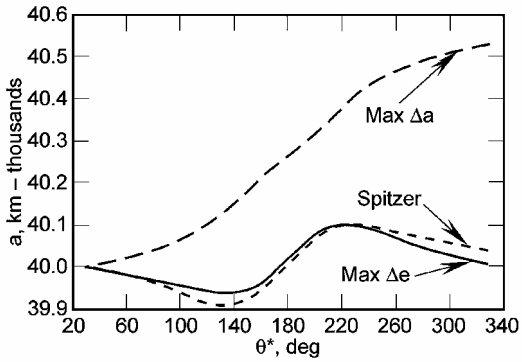

Fig. 3 Semimajor axis variation for maximum Δe, maximum Δa, and Spitzer[6,7] solutions.

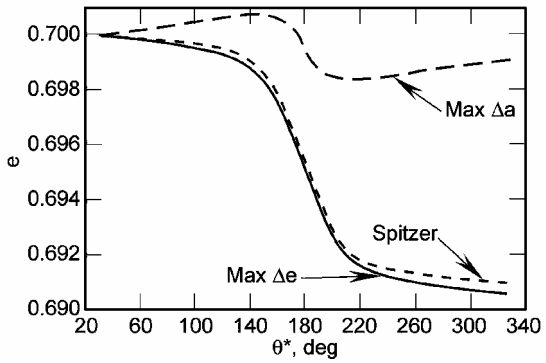

Fig. 4 Eccentricity variation for maximum Δe, maximum Δa, and Spitzer[6,7] solutions.

Table 2 Achieved final parameters with Δa-constrained, Δe-optimizing and Spitzer[6,7] modes for $\beta = 0$–150 deg

	β, deg					
Parameter	*0*	*30*	*60*	*90*	*120*	*150*
$(\lambda)_{\Delta e}$, 1/km	-0.25669812×10^{-5}	-0.24080373×10^{-5}	-0.60456815×10^{-6}	-0.2563464×10^{-6}	-0.2338952×10^{-7}	-0.11460911×10^{-6}
$(\Delta e)_{\Delta e}$	-0.80332152×10^{-2}	-0.87636901×10^{-2}	-0.94523115×10^{-2}	-0.9314426×10^{-2}	-0.9246776×10^{-2}	-0.96956425×10^{-2}
$(a_f)_{\Delta e}$, km	*39998.623*	*40002.482*	*39996.023*	*40005.449*	*39997.453*	*39997.334*
$(e_f)_{\Delta e}$	*0.691958845*	*0.691218603*	*0.690659402*	*0.690620353*	*0.690614399*	*0.690606069*
$(a_f)_s$, km	*39964.157*	*39985.214*	*40012.055*	*40026.495*	*40032.887*	*40035.272*
$(e_f)_s$	*0.692067423*	*0.691339135*	*0.690850669*	*0.690785068*	*0.69079769*	*0.690809371*

Table 3 Achieved final parameters with Δa-constrained, Δe-optimizing, and Spitzer modes for $\beta = 180$–330 deg

	β, deg					
Parameter	*180*	*210*	*240*	*270*	*300*	*330*
$(\lambda)_{\Delta e}$, 1/km	-0.4454532×10^{-6}	-0.11460911×10^{-6}	-0.2338952×10^{-7}	-0.2563464×10^{-6}	-0.60456815×10^{-6}	-0.24080373×10^{-5}
$(\Delta e)_{\Delta e}$	-0.90423093×10^{-2}	-0.96956425×10^{-2}	-0.9246776×10^{-2}	-0.9314426×10^{-2}	-0.94523115×10^{-2}	-0.87636901×10^{-2}
$(a_f)_{\Delta e}$, km	*40005.308*	*39997.334*	*39997.453*	*40005.449*	*39996.023*	*40002.482*
$(e_f)_{\Delta e}$	*0.690604847*	*0.690606069*	*0.690614399*	*0.690620353*	*0.69065940*	*0.691218603*
$(a_f)_s$, km	*40035.843*	*40035.272*	*40032.887*	*40026.495*	*40012.055*	*39985.214*
$(e_f)_s$	*0.69081291*	*0.690809371*	*0.690797699*	*0.690785068*	*0.690850669*	*0.691339135*

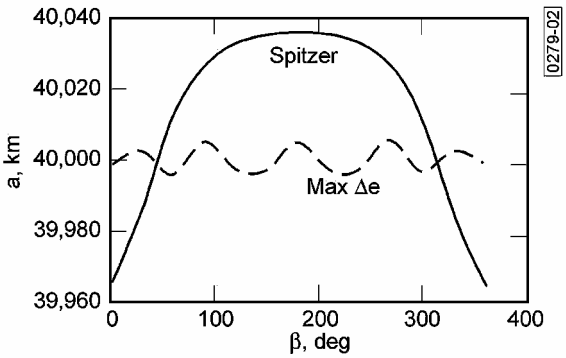

Fig. 5 Final achieved semimajor axis for maximum Δe and Spitzer[6,7] solutions as a function of sun angle β.

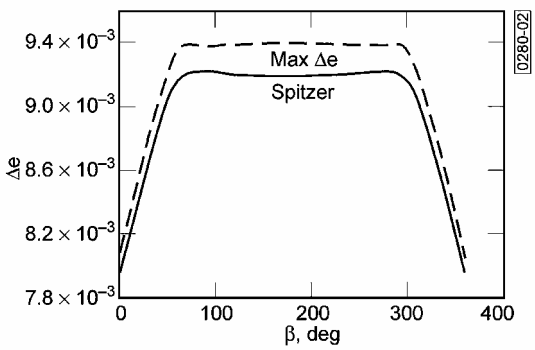

Fig. 6 Eccentricity change for maximum Δe and Spitzer[6,7] solutions as a function of sun angle β.

$(a_f)_{\Delta e}$ of the optimized solutions closely matching the 40,000-km constraint regardless of the value of β, whereas the Spitzer $(a_f)_s$ bell-shaped curve shows how the constraint is violated except for two narrow ranges centered around $\beta = 45$ and 315 deg.

Finally, in Fig. 6, the optimal Δe change as well as the Δe change of the Spitzer[6,7] solution are plotted vs β showing how the optimal solution yields the larger change as desired while also complying with the $\Delta a = 0$ constraint for this worst case of shadowing in this particular elliptic orbit example.

Analytic Integrations for the Spitzer Scheme

Because of the very low level of the low-thrust acceleration provided by the electric thrusters, it is possible to obtain analytic expressions for the changes experienced by the eccentricity and semimajor axis of a given orbit for the case where the constant thrust acceleration is applied in a fixed inertial orientation such as in the Spitzer[6,7] case. Because a and e vary by a small amount, after one cycle of thrust or an orbit, their value can be kept constant in the right-hand side of the variational equations, paving the way for their analytic integration.

Let us first start with the simplified equations of motion valid in circular orbit, which are obtained from Eqs. (6) and (7) by neglecting all terms of order e or higher:

$$\frac{\mathrm{d}a}{\mathrm{d}\theta^*} = 2k\frac{a^3}{\mu}s_\alpha \tag{21}$$

$$\frac{\mathrm{d}e}{\mathrm{d}\theta^*} = \frac{ka^2}{\mu}(c_\alpha s_{\theta^*} + 2s_\alpha c_{\theta^*}) \tag{22}$$

Using $s_\alpha = c_{\theta^*}$ and $c_\alpha = s_{\theta^*}$ (for increasing e), holding a as constant in the right-hand sides of Eqs. (21) and (22), and integrating between 0 and θ^* yields the simple expressions

$$a = a_0 + 2k(a^3/\mu)s_{\theta^*} \tag{23}$$

$$e = e_0 + (ka^2/\mu)\left(\tfrac{3}{2}\theta^* + s_{2\theta^*}/4\right) \tag{24}$$

An exact integration is also possible in this case. For instance, rewriting Eq. (21) as

$$a^{-3}\,\mathrm{d}a = 2(k/\mu)c_{\theta^*}\,\mathrm{d}\theta^*$$

and integrating results in the exact expression

$$a = a_0\left[1 - 4\left(ka_0^2/\mu\right)s_{\theta^*}\right]^{-\frac{1}{2}} \tag{25}$$

If this expression is now inserted in Eq. (22), then

$$e - e_0 = \frac{K}{4}\int_0^{\theta^*}\frac{\left(1 + c_{\theta^*}^2\right)}{(1 - Ks_{\theta^*})}\,\mathrm{d}\theta^*$$

where $K = 4ka_0^2/\mu$ is a constant and its value is less than one for typical low-thrust accelerations used in Earth orbit.

The first part of the preceding integral is easily obtained as

$$\int_0^{\theta^*}\frac{\mathrm{d}\theta^*}{(1 - Ks_{\theta^*})} = \frac{2}{(1 - K^2)^{\frac{1}{2}}}\tan^{-1}\left[\frac{\tan(\theta^*/2) - K}{(1 - K^2)^{\frac{1}{2}}}\right]\Bigg|_0^{\theta^*} \tag{26}$$

The second part is more complicated, and it is given by MATLAB® in the form

$$\frac{K}{4}\int_0^{\theta^*}\frac{c_{\theta^*}^2}{(1-Ks_{\theta^*})}\,\mathrm{d}\theta^* = -\frac{1}{2K}(1-K^2)^{\frac{1}{2}} \times \tan^{-1}\left[\frac{\tan(\theta^*/2)-K}{(1-K^2)^{\frac{1}{2}}}\right]\Bigg|_0^{\theta^*} + \frac{\theta^*}{4K}\Bigg|_0^{\theta^*} - \frac{1}{2}c_{\theta^*/2}^2\Bigg|_0^{\theta^*} \tag{27}$$

Therefore, a closed expression for e reads

$$e = e_0 + \frac{K}{2(1-K^2)^{\frac{1}{2}}}\tan^{-1}\left[\frac{\tan(\theta^*/2)-K}{(1-K^2)^{\frac{1}{2}}}\right]\Bigg|_0^{\theta^*} + \frac{\theta^*}{4K}\Bigg|_0^{\theta^*} - \frac{1}{2}c_{\theta^*/2}^2\Bigg|_0^{\theta^*} - \frac{1}{2K}(1-K^2)^{\frac{1}{2}}\tan^{-1}\left[\frac{\tan(\theta^*/2)-K}{(1-K^2)^{\frac{1}{2}}}\right]\Bigg|_0^{\theta^*} \tag{28}$$

The first and last inverse tangent terms can be combined into a single one; however, they are left that way because unlike the first one, the second inverse tangent term is very sensitive to small K when evaluated at $\theta^*=0$. For example, for $k=3.5\times10^{-7}$ km/s^2, $a_0=7000$ km, $e_0=0$, and $\mu=398601.3$ km^3/s^2, $K=1.72101796959\times10^{-4}$, $(1-K^2)^{1/2}=0.99999998519$ such that enough digits must be carried to prevent a less than precise calculation of e from Eq. (28), due to the already mentioned sensitivity. Also the proper branch of the inverse tangent function must be selected such that it corresponds to the one on which $\theta^*/2$ lies for any particular choice of θ^*. Otherwise, if the principal branch of the inverse tangent function is always employed in a systematic manner, then the answer will be wrong if the function does not represent the principal value. For example, for $\theta^*=220$ deg, then $\theta^*/2=110$ deg and the branch passing through $\theta^*=180$ deg must be selected, such that 180 deg must be added to the principal value for accurate evaluations. When these particular values of k, a_0, μ, and $\theta^*=220$ deg are used, Eqs. (23) and (25) yield $a=6999.6127813$ km and $a=6999.612845$ km, respectively, whereas Eqs. (24) and (28) yield $e=2.58401747\times10^{-4}$ and $e=2.58419725\times10^{-4}$.

The analytic integration of $\mathrm{d}a/\mathrm{d}\theta^*$ and $\mathrm{d}e/\mathrm{d}\theta^*$ in the elliptic case requires that a, e, and n be held constant in the right-hand sides of these differential equations, namely, Eqs. (6) and (7), which are rewritten for convenience:

$$\frac{\mathrm{d}a}{\mathrm{d}\theta^*} = \frac{2es_{\theta^*}(1-e^2)}{n^2(1+ec_{\theta^*})^2}kc_\alpha + \frac{2(1-e^2)}{n^2(1+ec_{\theta^*})}ks_\alpha \tag{29}$$

$$\frac{\mathrm{d}e}{\mathrm{d}\theta^*} = \frac{(1-e^2)^2 s_{\theta^*}}{n^2a(1+ec_{\theta^*})^2}kc_\alpha + \frac{(1-e^2)^2}{n^2ae}\left[\frac{1}{1+ec_{\theta^*}} - \frac{(1-e^2)}{(1+ec_{\theta^*}^3)}\right]ks_\alpha \tag{30}$$

For low-thrust acceleration, the assumption of holding a, e, and n constant is an excellent one with negligible effect on the final result when compared to the numerically integrated solution of the fully coupled preceding system over one cycle of thrust or a revolution. Let $c_\alpha=-s_{\theta^*}$ and $s_\alpha=-c_{\theta^*}$ for the Spitzer[6,7] scheme that reduces the orbital eccentricity after one cycle of thrust; then Eqs. (29) and (30) lead to

$$\int_{a_0}^{a}\mathrm{d}a = k_1\int_0^{\theta^*}\frac{s_{\theta^*}^2}{(1+ec_{\theta^*})^2}\,\mathrm{d}\theta^* + k_2\int_0^{\theta^*}\frac{c_{\theta^*}}{(1+ec_{\theta^*})}\,\mathrm{d}\theta^* \tag{31}$$

$$\int_{e_0}^{e}\mathrm{d}e = k_3\int_0^{\theta^*}\frac{s_{\theta^*}^2}{(1+ec_{\theta^*})^2}\,\mathrm{d}\theta^* + k_4\int_0^{\theta^*}\frac{c_{\theta^*}}{(1+ec_{\theta^*})}\,\mathrm{d}\theta^* + k_5\int_0^{\theta^*}\frac{c_{\theta^*}}{(1+ec_{\theta^*})^3}\,\mathrm{d}\theta^* \tag{32}$$

where $k_1=-2e(1-e^2)k/n^2$, $k_2=k_1/e$, $k_3=-(1-e^2)^2k/n^2a$, $k_4=k_3/e$, and $k_5=-k_4(1-e^2)=-(k_3/e)(1-e^2)$. The values of a and e are the initial values that correspond to $\theta^*=0$. The integrals involving $s_{\theta^*}^2$ are broken into two integrals after replacing $s_{\theta^*}^2=1-c_{\theta^*}^2$ such that the following integrals are needed:

$$\int\frac{\mathrm{d}\theta^*}{(1+ec_{\theta^*})^2}, \qquad \int\frac{c_{\theta^*}^2}{(1+ec_{\theta^*})^2}\,\mathrm{d}\theta^*$$

$$\int\frac{c_{\theta^*}}{(1+ec_{\theta^*})}\,\mathrm{d}\theta^*, \qquad \int\frac{c_{\theta^*}}{(1+ec_{\theta^*})^3}\,\mathrm{d}\theta^*$$

The first integral is solved through[11]

$$\int\frac{\mathrm{d}\theta^*}{(1+ec_{\theta^*})^2} = -\frac{es_{\theta^*}}{(1-e^2)(1+ec_{\theta^*})} + \frac{1}{(1-e^2)}\int\frac{\mathrm{d}\theta^*}{(1+ec_{\theta^*})} = \frac{-es_{\theta^*}}{(1-e^2)(1+ec_{\theta^*})} + \frac{2}{(1-e^2)^{\frac{3}{2}}}\tan^{-1}\left[\sqrt{\frac{1-e}{1+e}}\tan\frac{\theta^*}{2}\right] \tag{33}$$

Also

$$\int\frac{c_{\theta^*}}{(1+ec_{\theta^*})}\,\mathrm{d}\theta^* = \frac{\theta^*}{e} - \frac{1}{e}\int\frac{\mathrm{d}\theta^*}{(1+ec_{\theta^*})} = \frac{\theta^*}{e} - \frac{2}{e(1-e^2)^{\frac{1}{2}}} \times \tan^{-1}\left[\sqrt{\frac{1-e}{1+e}}\tan\frac{\theta^*}{2}\right] \tag{34}$$

Note that

$$\tan^{-1}\left[\sqrt{\frac{1-e}{1+e}}\tan\frac{\theta^*}{2}\right] = \frac{E}{2}$$

but that a more convenient expression relating θ^* and E is provided by,[12] namely, $\tan[(\theta^*-E)/2] = fs_E/(1-fc_E)$, where

$$f = \frac{(1+e)^{\frac{1}{2}} - (1-e)^{\frac{1}{2}}}{(1+e)^{\frac{1}{2}} + (1-e)^{\frac{1}{2}}}$$

leading to

$$\theta^* = E + 2\tan^{-1}\left[\frac{es_E}{1+(1-e^2)^{\frac{1}{2}} - ec_E}\right]$$

and conversely,

$$E = \theta^* - 2\tan^{-1}\left[\frac{es_{\theta^*}}{1+(1-e^2)^{\frac{1}{2}} + ec_{\theta^*}}\right]$$

which involve directly the sine and cosine of the angles E and θ^*.

Next, from the general form[11]

$$\int\frac{A+Bc_x}{(a+bc_x)^n}\,\mathrm{d}x = \frac{1}{(n-1)(a^2-b^2)}\left[\frac{(aB-Ab)s_x}{(a+bc_x)^{n-1}} + \int\frac{(Aa-bB)(n-1)+(n-2)(aB-bA)c_x}{(a+bc_x)^{n-1}}\,\mathrm{d}x\right]$$

we have

$$\int\frac{c_{\theta^*}}{(1+ec_{\theta^*})^3}\,\mathrm{d}\theta^* = \frac{s_{\theta^*}}{2(1-e^2)(1+ec_{\theta^*})^2} - \frac{e}{(1-e^2)} \times\int\frac{\mathrm{d}\theta^*}{(1+ec_{\theta^*})^2} + \frac{1}{2(1-e^2)}\int\frac{c_{\theta^*}}{(1+ec_{\theta^*})^2}\,\mathrm{d}\theta^* \tag{35}$$

The general form[11]

$$\int\frac{\mathrm{d}x}{(a+bc_x)^n} = -\frac{1}{(n-1)(a^2-b^2)} \times\left[\frac{bs_x}{(a+bc_x)^{n-1}} - \int\frac{(n-1)a-(n-2)bc_x}{(a+bc_x)^{n-1}}\,\mathrm{d}x\right]$$

provides

$$\int \frac{\mathrm{d}\theta^*}{(1+ec_{\theta^*})^2} = -\frac{es_{\theta^*}}{(1-e^2)(1+ec_{\theta^*})} + \frac{2}{(1-e^2)^{\frac{3}{2}}} \times \tan^{-1}\left[\sqrt{\frac{1-e}{1+e}}\tan\frac{\theta^*}{2}\right] \tag{36}$$

The general form immediately following Eq. (34) is used now to solve for

$$\int \frac{c_{\theta^*}}{(1+ec_{\theta^*})^2}\,\mathrm{d}\theta^* = \frac{s_{\theta^*}}{(1-e^2)(1+ec_{\theta^*})} - \frac{2e}{(1-e^2)^{\frac{3}{2}}} \times \tan^{-1}\left[\sqrt{\frac{1-e}{1+e}}\tan\frac{\theta^*}{2}\right] \tag{37}$$

and finally Eq. (35) is written as follows after adding the pertinent integrals:

$$\int \frac{c_{\theta^*}}{(1+ec_{\theta^*})^3}\,\mathrm{d}\theta^* = \frac{s_{\theta^*}\left[(1+ec_{\theta^*})(1+2e^2)+(1-e^2)\right]}{2(1-e^2)^2(1+ec_{\theta^*})^2} - \frac{3e}{(1-e^2)^{\frac{5}{2}}}\tan^{-1}\left[\sqrt{\frac{1-e}{1+e}}\tan\frac{\theta^*}{2}\right] \tag{38}$$

The final integral given next is obtained by way of symbolic integration using MALTAB:

$$\int \frac{c_{\theta^*}^2}{(1+ec_{\theta^*})^2}\,\mathrm{d}\theta^* = \frac{2(2e^2-1)}{e^2(1-e)^{\frac{3}{2}}}\tan^{-1}\left[\sqrt{\frac{1-e}{1+e}}\tan\frac{\theta^*}{2}\right] - \frac{s_{\theta^*}}{e(1-e^2)(1+ec_{\theta^*})} + \frac{\theta^*}{e^2} \tag{39}$$

Equation (31) can now readily be integrated to yield, after regrouping terms, the following analytic expression for $\Delta a = a - a_0$:

$$\Delta a = \left.\frac{k_1 s_{\theta^*}}{e(1+ec_{\theta^*})}\right|_0^{\theta^*}, \qquad k_1 = -2e(1-e^2)\frac{k}{n^2} \tag{40}$$

As e approaches zero and with k_1 being linear in e, Eq. (40) reduces to

$$\Delta a = -(2k/n^2)s_{\theta^*}|_0^{\theta^*}$$

which is identical to the simple expression in Eq. (23) except for the minus sign because here we used $s_\alpha = -c_{\theta^*}$ and $c_\alpha = -s_{\theta^*}$ to reduce eccentricity as opposed to Eq. (23), which was obtained with $s_\alpha = c_{\theta^*}$ and $c_\alpha = s_{\theta^*}$ firing in the reverse direction to increase eccentricity.

The integration of Eq. (32) is also carried out to yield after regrouping terms the following analytic expression for $\Delta e = e - e_0$, as a function of θ^*, valid in general elliptic orbit:

$$\Delta e = \left.\frac{(1+ec_{\theta^*})(1-4e^2)-(1-e^2)}{2e(1-e^2)(1+ec_{\theta^*})^2}k_3 s_{\theta^*}\right|_0^{\theta^*} + \left.\frac{3k_3}{(1-e^2)^{\frac{3}{2}}}\tan^{-1}\left[\sqrt{\frac{1-e}{1+e}}\tan\frac{\theta^*}{2}\right]\right|_0^{\theta^*}$$

$$k_3 = -\frac{(1-e^2)^2 k}{n^2 a} \tag{41}$$

For small e, the leading term in $(1+ec_{\theta^*})(1-4e^2)-(1-e^2)$ is ec_{θ^*} such that, as e approaches zero, Eq. (41) collapses to

$$\Delta e = \left.-\frac{k}{n^2 a}\frac{s_{2\theta^*}}{4}\right|_0^{\theta^*} - \left.\frac{3k}{2n^2 a}\theta^*\right|_0^{\theta^*}$$

identical to Eq. (24) except once again for the change in the sign because of the reversed firing orientation as compared to the direction assumed in Eq. (24). Thus, both expressions for a and e in Eqs. (40) and (41) valid in the general elliptic case reduce to the simpler expressions in Eqs. (23) and (24) when e tends to zero, providing a good check. The integration limits can of course be any two true anomaly values and not necessarily 0 and the general θ^* values. The values of a and e appearing in the right-hand sides of all of the equations derived in this paper correspond to the initial values a_0 and e_0. The subscript zero was left out for ease of writing purposes. When $a_0 = 40{,}000$ km, $e_0 = 0.7$, and the same values of $\mu = 398{,}601.3$ km^3/s^2 and $k = 3.5 \times 10^{-7}$ km/s^2 are used as before, the numerical integration of Eqs. (29) and (30) with $a = a_0$ and $e = e_0$ held constant in the right-hand sides during integration between the bounds $\theta_0^* = 30.1286983$ deg and $\theta_f^* = 329.871302$ deg, which correspond to the case of $\beta = 180$ deg in Table 1, yield $a_f = 40{,}035.8429$ km and $e_f = 0.6908129217$ for the Spitzer[6,7] e-drop strategy. Equations (40) and (41) yield $\Delta a = 35.842917$ km and $\Delta e = -9.18707831 \times 10^{-3}$, respectively, or $a_f = 40{,}035.842917$ km and $e_f = 0.690812922$, which are identical to the numerically integrated values, thereby validating the analytic expressions derived here. Finally, these analytic integrations are related to the exact analytic elliptic integrals in Cartesian coordinates[13] for the case of thrust oriented in a constant inertial direction.

Conclusions

The maximization of the change in the eccentricity of a general elliptic orbit subject to the constraint of zero change in the semimajor axis while in the presence of a shadow arc where no thrust is applied is carried out by direct application of the theory of maxima. The method is also applied to the dual problem of maximizing the orbital energy while keeping eccentricity unchanged. A typical high-energy, high-eccentricity orbit is used as an example, and the worst case of shadowing geometry, which takes place when the sun–Earth line is contained in the spacecraft orbit plane, is selected to compare the achieved optimal changes in the eccentricity for various sun angles to the suboptimal results obtained with the simpler fixed firing orientation scheme. Furthermore, analytic expressions for the changes in the semimajor axis and eccentricity resulting from the latter firing mode are also derived in the general elliptic case.

References

[1] Edelbaum, T. N., "Propulsion Requirements for Controllable Satellites," *ARS Journal*, Aug. 1961, pp. 1079–1089.

[2] Cass, J. R., "Discontinuous Low Thrust Orbit Transfer," M.S. Thesis, School of Engineering, U.S. Air Force Inst. of Technology, Rept. AFIT/GA/AA/83D-1, Wright–Patterson AFB, OH, Dec. 1983.

[3] McCann, J. M., "Optimal Launch Time for a Discontinuous Low Thrust Orbit Transfer," M.S. Thesis, School of Engineering, U.S. Air Force Inst. of Technology, Rept. AFIT/GA/AA/88D-7, Wright–Patterson AFB, OH, Dec. 1988.

[4] Kéchichian, J. A., "Low-Thrust Eccentricity-Constrained Orbit Raising," *Journal of Spacecraft and Rockets*, Vol. 35, No. 3, 1998, pp. 327–335.

[5] Burt, E. G. C., "On Space Maneuvers with Continuous Thrust," *Planetary and Space Science*, Vol. 15, 1967, pp. 103–122.

[6] Spitzer, A., "Near Optimal Transfer Orbit Trajectory Using Electric Propulsion," American Astronautical Society, AAS Paper 95-215, Feb. 1995.

[7] Spitzer, A., "Novel Orbit Raising Strategy Makes Low Thrust Commercially Viable," 24th International Electric Propulsion Conf., IEPC Paper 95-212, Sept. 1995.

[8] Kéchichian, J. A., "Optimum Thrust Pitch Profiles for Certain Orbit Control Problems," *Journal of Spacecraft and Rockets*, Vol. 40, No. 2, 2003, pp. 253–259.

[9] Battin, R. H., *An Introduction to the Mathematics and Methods of Astrodynamics*, AIAA Education Series, AIAA, New York, 1987, pp. 128, 488.

[10] Press, W. H., Flannery, B. P., Teukolsky, S. A., and Vetterling, W. T., *Numerical Recipes (Fortran)*, Cambridge Univ. Press, Cambridge, England, U.K., 1989, pp. 251–254.

[11] Gradshteyn, I. S., and Ryzhik, I. M., *Table of Integrals, Series, and Products*, Academic Press, New York, 1980.

[12] Wintner, A., "The Analytical Foundation of Celestial Mechanics," Princeton Univ. Press, Princeton, NJ, 1947, pp. 201–210.

[13] Grodzovskii, G. L., Ivanov, Y. N., and Tokarev, V. V., "Mechanics of Low-Thrust Spaceflight," translated by A. Baruch, edited by Y. M. Timant, NASA TTF-507, TT 68-50301, Israel Program for Scientific Translation, Jerusalem, 1969, pp. 431, 432 (translated from Russian).